Implementation of Petrographical and Aeromagnetic Data to Determine Depth and Structural Trend of Homrit Waggat Area, Central Eastern Desert, Egypt

El Saeed R. Lasheen [1], Waheed H. Mohamed [1], Antoaneta Ene [2,*], Hamdy A. Awad [3,*] and Mokhles K. Azer [4]

1   Geology Department, Faculty of Science, Al-Azhar University, Cairo 11884, Egypt
2   INPOLDE Research Center, Department of Chemistry, Physics and Environment, Faculty of Sciences and Environment, Dunarea de Jos University of Galati, 47 Domneasca Street, 800008 Galati, Romania
3   Geology Department, Faculty of Science, Al-Azhar University, Assiut Branch, Assiut 71524, Egypt
4   Geological Sciences Department, National Research Centre, Dokki, Giza 12622, Egypt
*   Correspondence: antoaneta.ene@ugal.ro (A.E.); hamdiawaad@gmail.com (H.A.A.)

Abstract: In the current study, we conducted petrographic investigation combined with aeromagnetic data in order to classify variable granitic rocks, delineate structural trends and deduce depth of the basement rocks cropping out in Homrit Waggat area, Central Eastern Desert, Egypt. Field and petrographic investigations revealed that the granitic Homrit Waggat rocks include two groups. The first group includes the older granitic rocks, comprising tonalites and granodiorites. In contrast, the second one includes younger granitic rocks, involving alkali-feldspar granites, syenogranites and albitized granites. Depth as well as subsurface structures can be identified using magnetic method. Two tectonic maps representing the deep-seated and the shallow-seated structural features were constructed to show the structural history of the study area. The major tectonic trends indicate that the regional structures are controlled by deeper structures which have NW–SE, NNE–SSW—NE–SW and N–S directions. On the other hand, we find that the local structure trends are controlled by the local shallow structures that have NNE–SSW, NNW–SSE, ESE–WNW and N–S directions. Depth levels of the economic rare metal-bearing rocks range from 0 km to 1.2 km (Euler deconvolution technique) and from 0 km to 2.3 km (the analytical signal profiles) by using the aeromagnetic data, reflecting large resources of rare metal-bearing rocks.

Keywords: aeromagnetic; analytical signal; structure; petrographic; Homrit Waggat

1. Introduction

Cryogenian–Ediacaran granitic rocks are widely distributed in the Northern corner of the Arabian-Nubian Shield (ANS) [1–3]. ANS represents one of the largest continental crusts (after collision of East and West Gondwana), formed by accretionary terrane [4–7]. The ANS crops out in the Eastern Desert, South Sinai as well as in the southern corner of the Western Desert, and comprises Neoproterozoic Island arc assemblages overthrusted by ophiolitic rocks and injected by variable granitic rocks.

Among the Neoproterozoic Egyptian rocks, the highly evolved (fractionated) granitic rocks are accompanied by rare metals mineralization [2,8–10]. They possess high contents of rare metals such as Nb, Ta, Y, Sn, Zr, REEs and highly radioactive mineralization [11–13]. These granitic bodies are abundant in the Northern and Central Eastern Desert (CED) of Egypt with varying shapes and reliefs. They are characterized by enrichment in REEs, Nb, Ta, U, Th, Zr and the high content in total alkalis may be related to magmatic and/or hydrothermal alterations [9,14].

The highest contents of rare metal-bearing granitic rocks cropping out in the Egyptian Eastern Desert are Nuweibi, Homrit Waggat, Abu Dabbab, Abu Diab, Abu Rusheid and Gattar granitic intrusions [9,15]. Moreover, plutonic rocks including granites due to their

abundance (60% of the total Egyptian crystalline rocks) are widely utilized as an ornamental stone due to high durability as well as good appearance [2].

The aeromagnetic survey is a helpful technique for geological mapping as it provides information at a fraction of the cost of ground mapping. One of the major purposes of the aeromagnetic survey is to distinguish the relationship between magnetic anomalies and tectonic pattern that is typically present in survey areas. This is because magnetic anomalies preserve the tectonic history of the rocks by their magnitude and pattern. As a result, any extensive magnetic measurements will contain anomalies with a non-random pattern.

A magnetic survey is widely used to examine the subsurface anomalies caused by the magnetic characteristics of the underlying rocks. Magnetic content (susceptibility) of rocks varies depending on the type of rock and the environment in which it is found. The texture of the anomaly field is the trends, sizes, and configurations of the numerous anomaly centers; the presence of shape gradients is the most important aspect in the interpretation of aeromagnetic maps [16]. The susceptibility, geometry, depth of burial, remnant magnetization, striking direction, and local magnetic inclination and declination all influence the form and magnitude of a magnetic anomaly. Changes in these factors, within and between rock types, give the aeromagnetic map particular distinguishing characteristics that reflect the underlying geology.

The current work aims to investigate and classify the various Homrit Waggat granitic rocks through petrographical investigation, evaluate the subsurface structure affecting the studied area and determine their depth using aeromagnetic method.

2. Geologic Setting

The heterogenity of the Egyptian granitic rocks is due to variation in their mineralogical and geochemical compositions [9,10]. Therefore, they comprise two main rock types. The first is the older group characterized by grey color, calc-alkaline and I-type plutonic rocks (850–614 Ma), whereas the pink (younger) granite is the second type [17]. Younger granites range from calc alkaline (volcanic arc monzogranites) to alkaine (within plate setting) affinity.

The Egyptian younger granitic rocks are abundant in the Northeastern Desert relative to the Central and Southeastern Desert [9], whereas the older ones decrease from southern to northern sectors of the Eastern Desert [9]. The Homrit Waggat area lies in the Central Eastern Desert (Figure 1a), Northwest Mersa Alam. A lensoid (discontinued ring) shape of low to intermediate relief is the general habit of Homrit Waggat intrusions (Figure 1b). They mainly comprise multi magmatic phases (grey to pink granites). Grey granites are characterized by elliptical, exfoliated forming low hills. They are fine-grained and cut by quartz veins and pegmatites. In contrast, the younger rocks are predominant in the studied area covering an area of approximately 50 km^2 [11,12]. They are characterized by pink color (Figure 2), contain xenoliths from the older rocks and are cavernous. They are intruded by pegmatite and quartz veins of varying size. In addition, volcano-sedimentary as well as a metagabbro-diorite complexes are the oldest rock units forming the Northern part of the area under investigation.
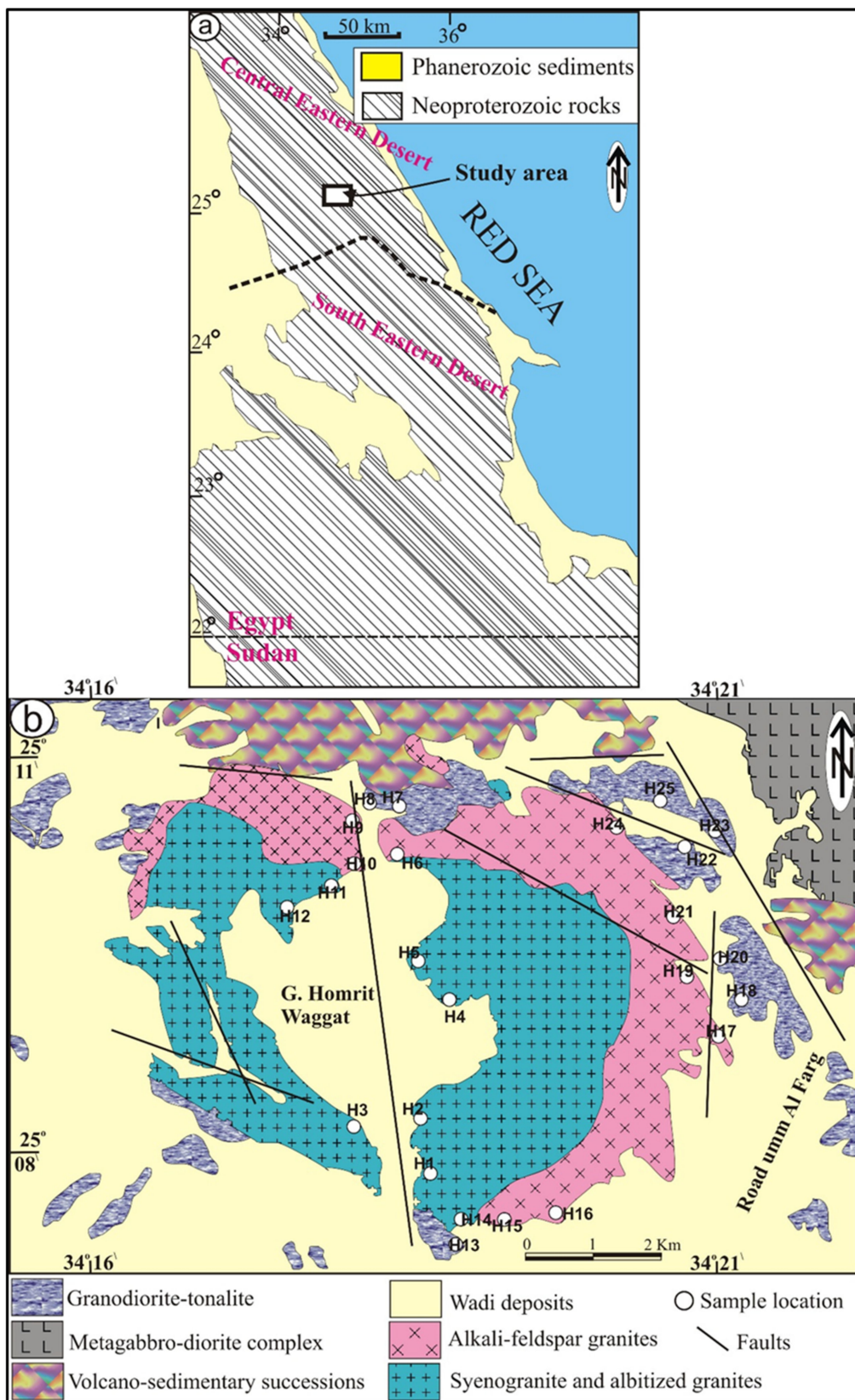
Figure 1. (**a**) Location map of Homrit Waggat area, Central Eastern Desert of Egypt; (**b**) geologic map of Homrit Waggat area with sample locations modified after [11,12].
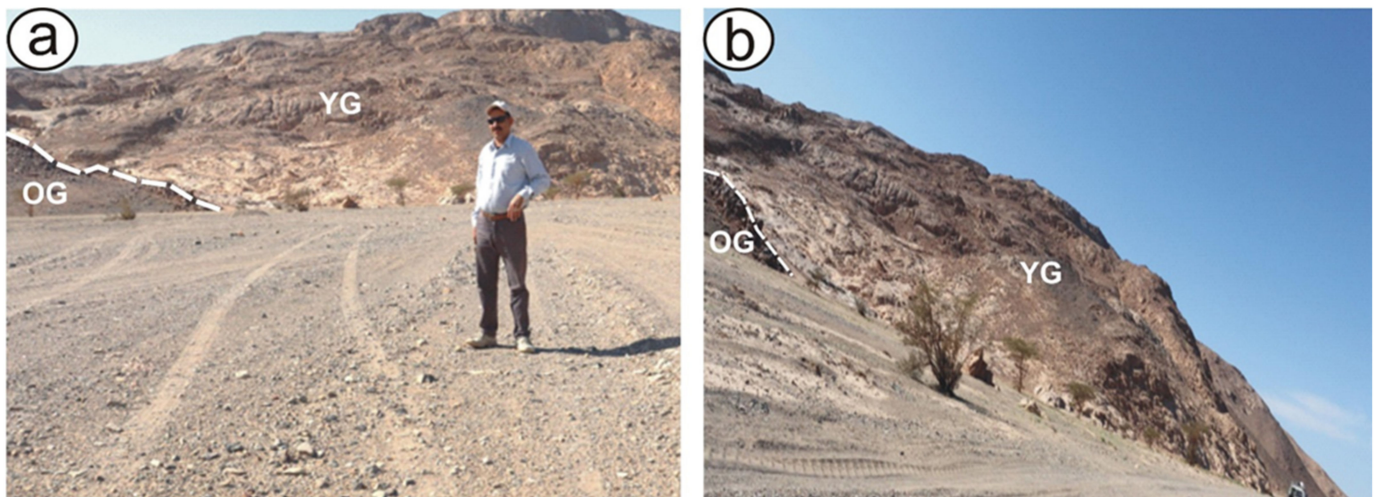
Figure 2. Field photographs showing general views of Homrit Waggat area from its core, revealing the contact between older granitic (OG) rocks and younger granites (YG).

3. Materials and Methods

A total of 25 samples were collected from the studied area, from which 15 samples were selected for petrographical study by polarizing microscope (Olympus bx53). We provided petrographical investigation for the area under investigation in order to identify the variable rock types.

The airborne magnetic data used in this study were obtained as part of the airborne spectrometric/magnetic survey flown and compiled in 1984 by the Aero-Service Division. A Varian V-85 proton free-precession magnetometer with a sensitivity of 0.1 nT was employed during the survey as a low-sensitivity airborne magnetometer. The magnetometer was installed in the aircraft's fibreglass tail stinger. A Varian VIW 2321 G4 magnetometer was used as a base station magnetometer. This survey was carried out in parallel flight lines with NE–SW orientation at spacing of 1.0 km between the flight lines. The obtained data were corrected and plotted as total aeromagnetic intensity map. In this study, the digitizing process follows the basic acquired analog data flight lines drawn on the map and the obtained data are shown as filled colors of the total magnetic map. Different processing methods were applied to the aeromagnetic data using Geosoft oasis montaj software. The processing in this study was preliminarly carried out by reduction of the magnetic northern pole (RTP). The filters technique (regional andresidual filters) was used in the interpretation and delineation of shallow and deep subsurface structures of the studied area. In this study, several advanced techniques were used to analyze the magnetic data as a guide for structural interpretation and basement configuration. These methods are analytical signal and Euler deconvolution methods and are proven as efficient tools to calculate the basement depth and location of magnetic structures such as faults or contacts.

4. Results and Discussion

4.1. Petrographical Examination

The Homrit Waggat area comprises several granitic rocks according to their mineralogical composition. They include older granites (tonalite and granodiorite) and younger granites (syenogranite, alkali-feldspar granite, and albitized granite).

Tonalite is medium-grained (2–4 mm) and characterized by hypidiomorphic texture. It is composed essentially of plagioclase, quartz, as well as hornblende with traces (or minor) of K-feldspar. Plagioclase occurs as subhedral crystals that exhibit moderate to extensive turbidity surface because of saussuritization processes (Figure 3a). Thus, their twinning is extinct. Quartz exhibits undulose extinction and occurs in two generations (fine- to medium-grained). Relics of hornblende are recorded due to extensive chloritization. Perthitetexture is abundant with a clear worm-like shape,
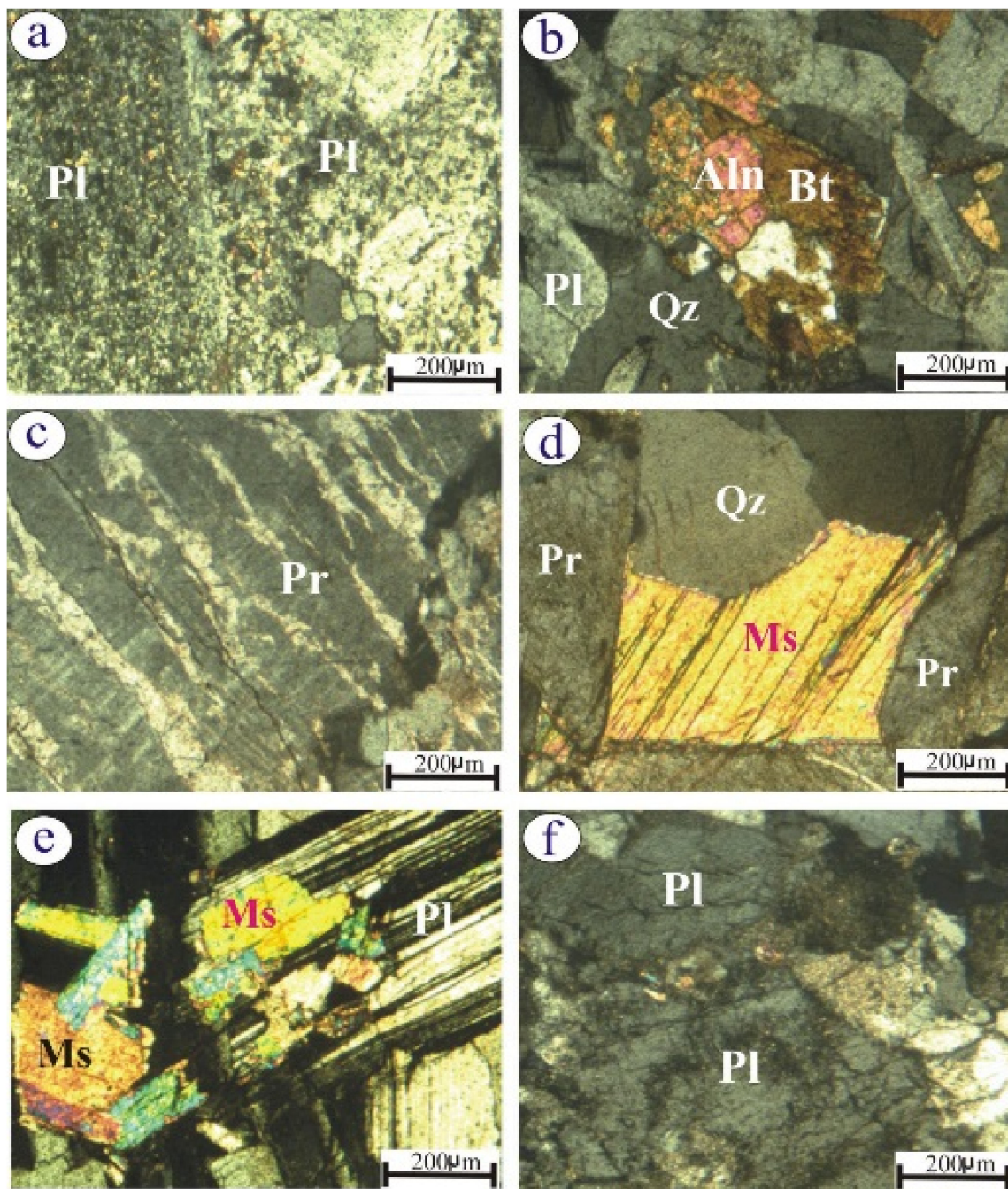
Figure 3. Crossed-polar photomicrographs showing (**a**) Extensive plagioclase saussiritization (Pl) in tonalite; (**b**) Allanite (Aln) associated with biotite (Bt) crystals in granodiorite; (**c**) Pristine patchy perthite (Pr) in syenogranite; (**d**) Coarse-grained muscovite (Ms) associated with perthite and quartz (Qz) in alkali-feldspar granites; (**e**) Coarse-grained plagioclase engulfing fine-grained muscovite in alkali-feldspar granites; and (**f**) Turbid albite plagioclase crystals in albitite granites.

Granodiorite is medium-grained (2–4 mm) and consists mainly of plagioclase, K-feldspar, quartz, and biotite as major minerals, whereas allanite, titanite and zircon are the main accessory minerals. Plagioclase occurs as tabular crystals exhibiting both lamellar and zoned twinning. It shows a slightly turbid surface because of alteration (kaolinitization) processes. Patchy perthite (intergrowth texture between K-feldspar and albite) occurs commonly enclosing small plagioclase crystals. Quartz is present as fine- to medium-grained crystals. Flaky biotite crystals are partially altered to chlorite. Titanite occurs as

wedge-shaped crystals. Moreover, allanite is present as reddish-brown crystal associated with biotite crystals (Figure 3b).

Syenogranite is coarse-grained (>5 mm), composed mainly of quartz, K-feldspar, and plagioclase as major minerals. Zircon and iron oxide (hematite) are the main accessory phases. These rocks exhibit hypidiomorphic textures. Quartz shows normal extinction and occasionally is engulfed in plagioclase crystals. Microcline shows clear crosshatching. Orthoclase-perthite is abundant with simple twinning (Figure 3c) and is either pristine or slightly kaolinitized. Moreover, biotite crystals (flaky) are partially altered to chlorite forming rims. Zircon crystals are disseminated and enclosed in other minerals such as biotite.

Alkali-feldspar granites are coarse-grained (>6 mm), comprising mainly quartz, K-feldspars, plagioclase, and muscovite. Quartz crystals are fine- to medium-grained and show normal extinction. Flamy as well as patchy perthitic textures are recorded. Subhedral crystals of plagioclase reveal slight saussuritization. Fine- to coarse-grained muscovite crystals with clear cleavage are present (Figure 3d,e).

Albitic granites are fine-grained (<1 mm), have a white color and comprise albite and quartz crystals with minor K-feldspar. Albite forms subhedral and tabular grains that are rarely fractured. It reveals a completely turbid surface as a result of kaolinitization process (Figure 3f). Quartz occurs as anhedral crystals with normal extinction. K-feldspar occurs as fine-grained perthite crystals. Zircon is the main accessory mineral with pleochroic haloes and is commonly enclosed in albite.

4.2. Airborne Magnetic Data

Magnetic anomalies are caused by the presence of magnetic minerals in both surface and subsurface rocks. These anomalies can be shown in maps reflecting the geology of the area under investigations [18]. The Egyptian General Petroleum Corporation provided the total field magnetic anomaly maps used in this investigation. Variable anomalies (long and short wavelengths) may be found on the aeromagnetic maps (Figure 4). Therefore, they are utilized to define the reduced pole (RTP) of an aeromagnetic map (Figure 5), allowing the shape and peak of magnetic anomalies above their generating bodies to be corrected. The International Geomagnetic Reference Field (IGRF-42425) was firstly removed from the data. For the analysis of magnetic anomalies the RTP data were employed. Using the Magmap tool of Geosoft, Oasis Montaj software, the RTP correction assumed $1.9°$ declination and $32.8°$ inclination for the area under investigation [19–21].

4.3. Reduction to the North Magnetic Pole Map

Due to the inclination of the Earth's magnetic field, most magnetic anomalies have both a positive and negative effect. These minima and maxima are frequently offset from the producing body along the magnetic meridian. When the inclination is 90 degrees, the magnetic anomaly is located right above the source body's centre. To remove these effects, the reduction to the pole (RTP) approach is utilised, which makes the data look as if they were taken at the pole, where the magnetic field is practically vertical. The magnetic maxima, in turn, occurs directly over the magnetised objects, notably when remnant magnetization is absent [22]. According to Blakely [23], the field reduced to the pole at a fixed point above the measurement plane in frequency domain is given by

$$L(\theta) = 1/[\sin(I\alpha) - i\cos(I)\cos(D + \theta)]^2, \text{ if } (I\alpha < I), I\alpha = I$$

where I = geomagnetic inclination, Iα = inclination for amplitude correction, D = geomagnetic declination, θ = wavenumber direction, i = imaginary component.
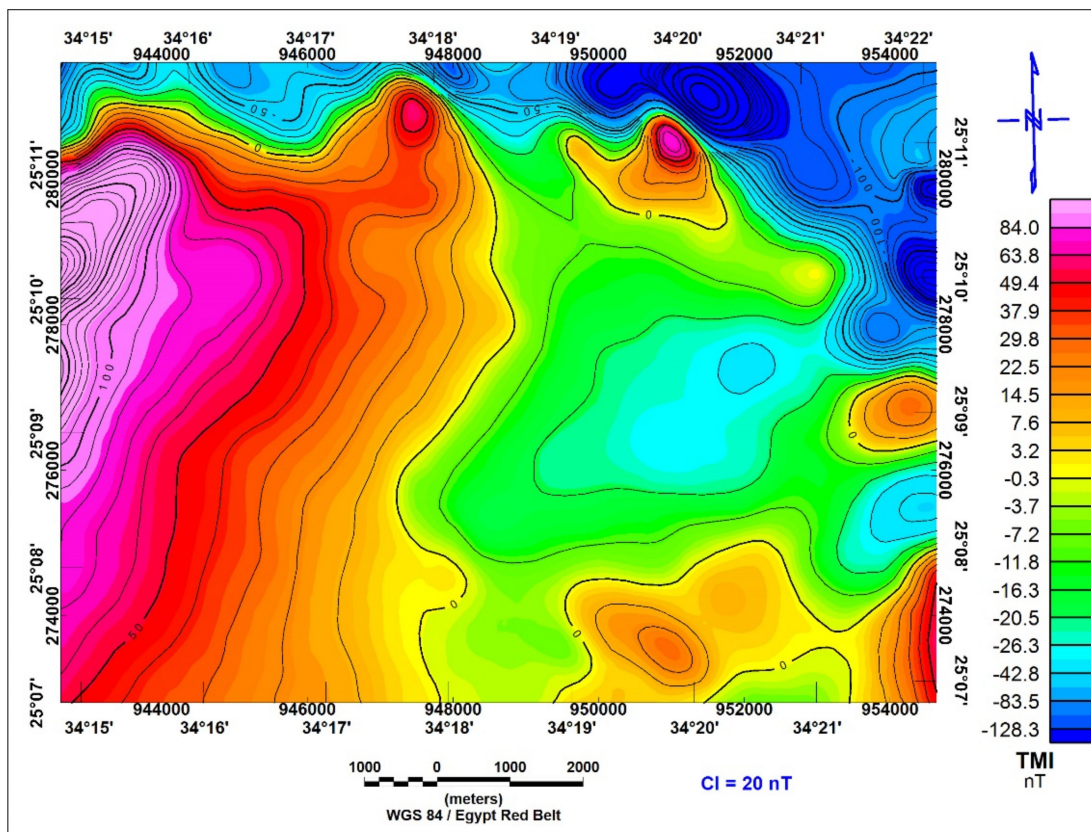
Figure 4. Total-airborne magnetic-field anomaly (TMA) map of Homrit Waggat area [21].
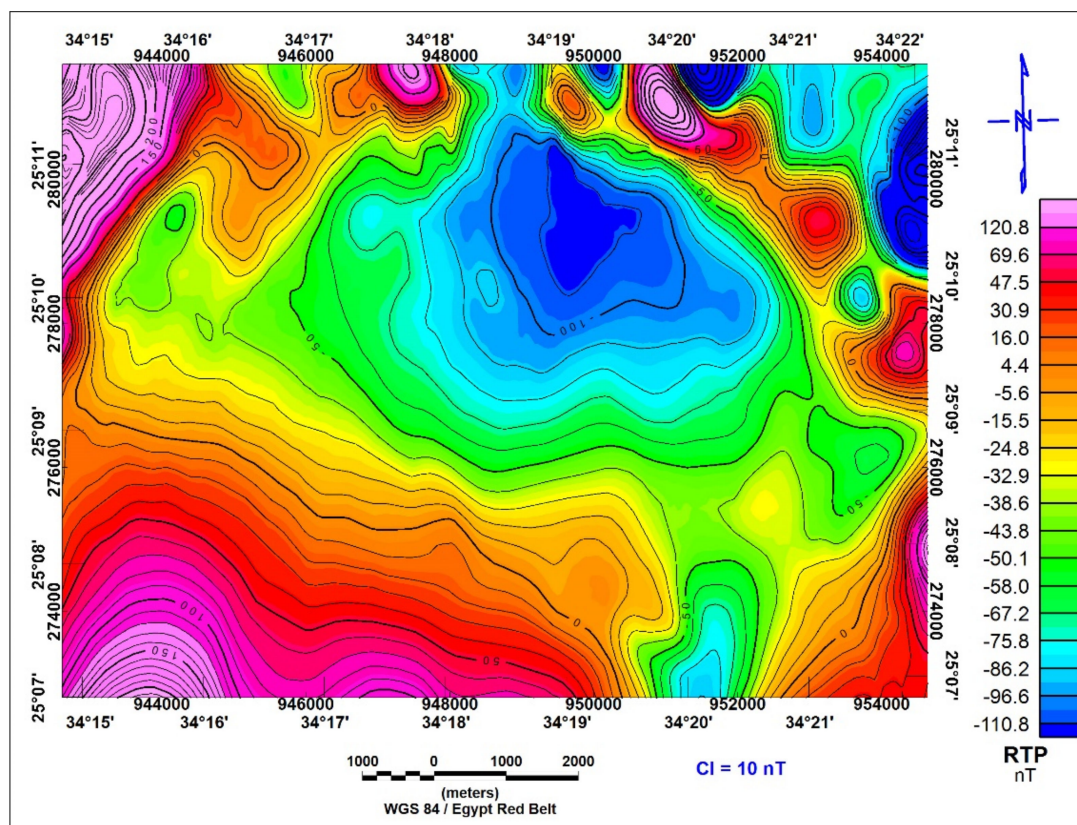

Figure 5. Reduced to the north magnetic pole (RTP) map of Homrit Waggat area.

The RTP field (Figure 5) illustrates a large positive magnetic zone of anomaly with different amplitudes, ranging between 0 nT and 120 nT, trending towards the NE and NW directions. It is located in different points of the study area. This anomaly represents the highest amplitude within the study area, reflecting the granodiorite-tonalite associations. Meanwhile, the central and northeastern parts of the map are occupied by a NW–SE magnetic belt. This belt illustrates an intermediate and low magnetic anomaly with relative amplitudes, ranging between 0 nT and −110 nT. This is probably associated with the metagabbro-diorite complex, syenogranite and albitized granites.

4.4. Regional Magnetic Anomaly Map

The Gaussian filler technique is used to distinguish broad "regional" variations from sharper "local" variations in magnetic anomalies. To put it in another way, the magnetic map is split into two parts, the regional and the residual magnetic component maps.

The regional magnetic anomaly map shows that the vertical magnetic components decrease in the central and northeastern portion of the studied area (Figure 6). The magnetic properties in these parts reflect the wadi deposit, the alkali-feldspar granites and syenogranites, albitized granites and metagabbro-diorite complex features. The shape of the negative anomaly is semicircular while its sharpness is smooth and reflects deep magnetic sources. Alternatively, the eastern and western parts exhibit two broad zones of high magnetization that are clearly expressed in the regional map. In addition, the anomaly trends seem to be affected by different stresses, as determined from prominent directions, namely the NW–SE and NE–SW, and their relative strength is closely related to the duration and magnitude of the affecting forces.
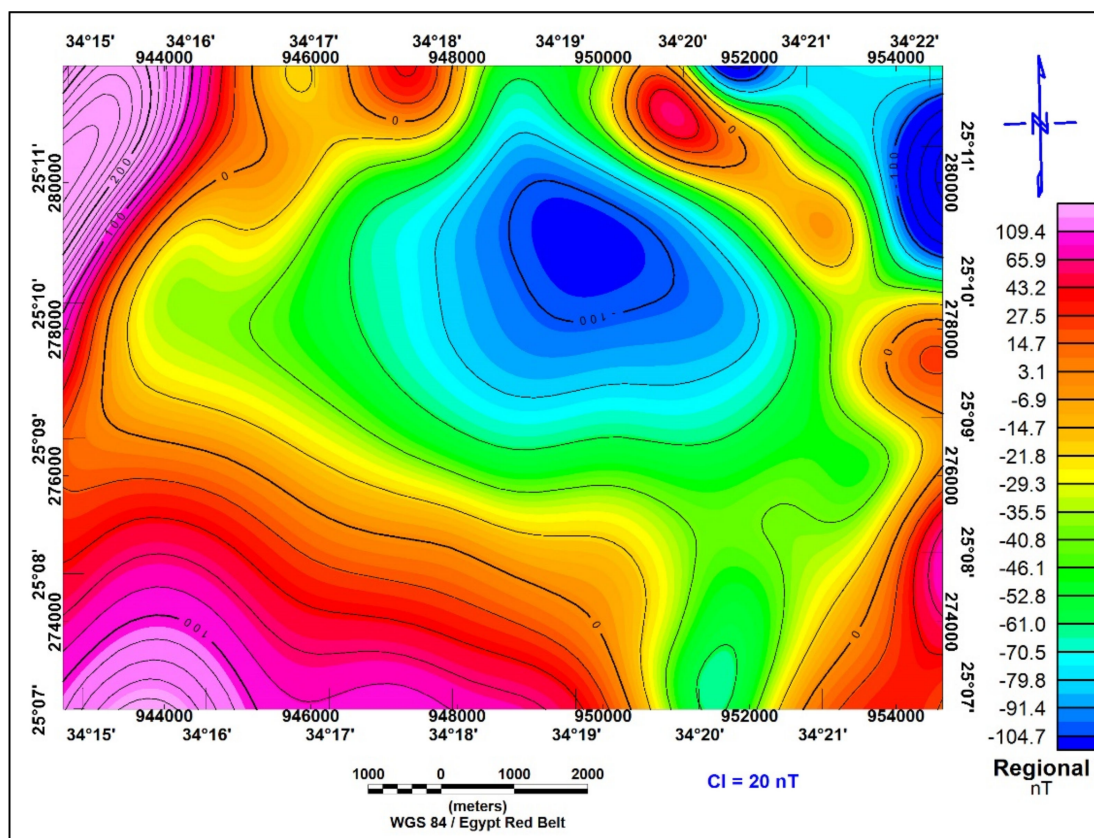

Figure 6. Regional airborne magnetic component of the RTP map of Homrit Waggat.

4.5. Residual Magnetic Anomaly Map

Geophysicists have employed residual aerial magnetic maps to distinguish local structures that are often confounded by larger field phenomena [24]. Residual map construction

represents one of the best ways to study a potential map quantitatively, where the measured field includes effects from all bodies in the vicinity. The residual anomaly focuses on weaker features that are confused by strong deep-seated effects in the original map [25]. The residual or near magnetic component map (Figure 7) seems to be noisier than the original magnetic map and characterized by high-frequency anomalies of small size, weak intensity, and sharp amplitudes. Positive and negative local anomalies might suggest the presence of fault structures in the form of highlands and lowlands. The filtered maps reveal complex structures in some areas, maybe due to susceptibility contrast or, more likely, highly magnetic causative sources. The residual magnetic anomalies show four major orientations of N–S, NNW–SSE, NW–SE, and NE–SW directions. Consequently, the stresses affected on the near-surface constituents are somewhat different from the deep-seated ones.
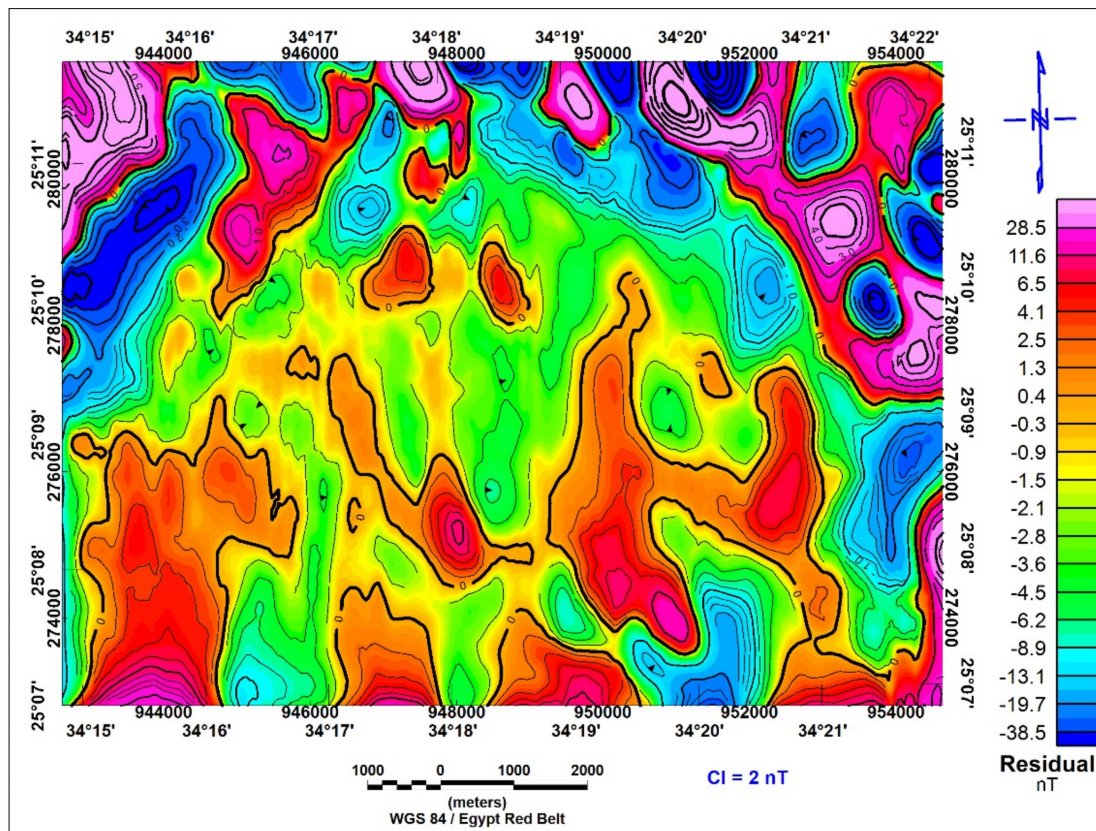

Figure 7. Residual airborne magnetic component of the RTP map of Homrit Waggat area.

4.6. Analytical Signal Technique

Analytical signal is a well-known gradient enhancement that is connected to magnetic fields using derivatives. Roest et al. [21] stated that the first analytical signal amplitude can be calculated using three orthogonal gradients of the total magnetic field through the expression:

$$|A(x,y)| = \sqrt{\left(\left(\frac{\delta m^2}{\delta x} \right) + \left(\frac{\delta m^2}{\delta y} \right) + \left(\frac{\delta m^2}{\delta z} \right) \right)}$$

where $A(x,y)$ is the amplitude of the analytical signal at (x,y), and m is the observed magnetic anomaly at (x,y). While this function is not a measurable parameter, it is extremely useful in terms of interpretation because it is totally independent of magnetization and the direction of the Earth's field [26]. As a result, all bodies with the same shape have the same analytical signal. Figure 8 illustrates the three analytical signal profiles (P1-P1↘, P2-P2↘ and P3-P3↘) above the map reduced to magnetic pole. The first analytical signal profile P1-P1↘ (Figure 9) is about 9065 m long and cuts the western portion of the study area in a NNE–SSW direction.

The depths of the basement surface range from 0 to 2000 m. The second analytical signal profile P2-P2$^\searrow$ (Figure 10) is about 10,570 m long and cuts the eastern portion of the study area in a NE–SW direction. The depths of the basement surface along this profile range from 0 m to 2300 m. The third analytical signal profile P3-P3$^\searrow$ (Figure 11) is about 15,120 m long and cuts the central portion of the study area in a NW–SE direction. The depths of the basement surface along this profile range from 0 m to 2300 m.
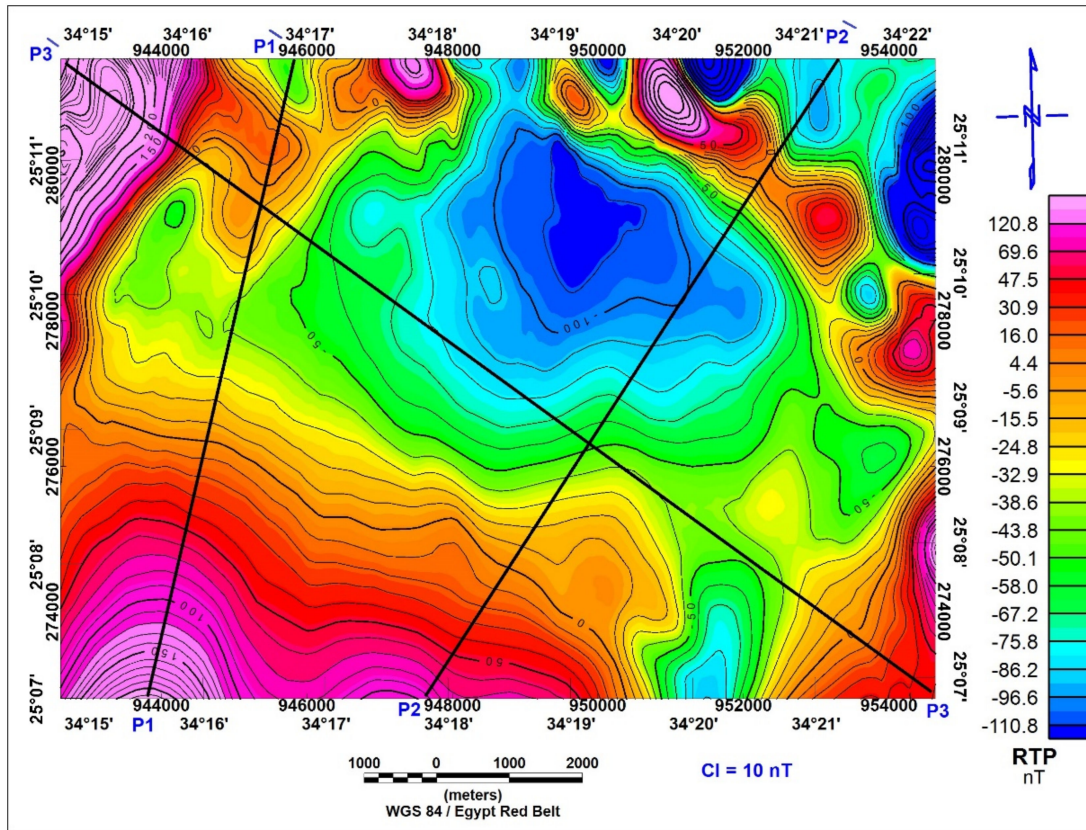

Figure 8. RTP aeromagnetic anomaly map of the studied area showing the profiles used for application of analytical signal.
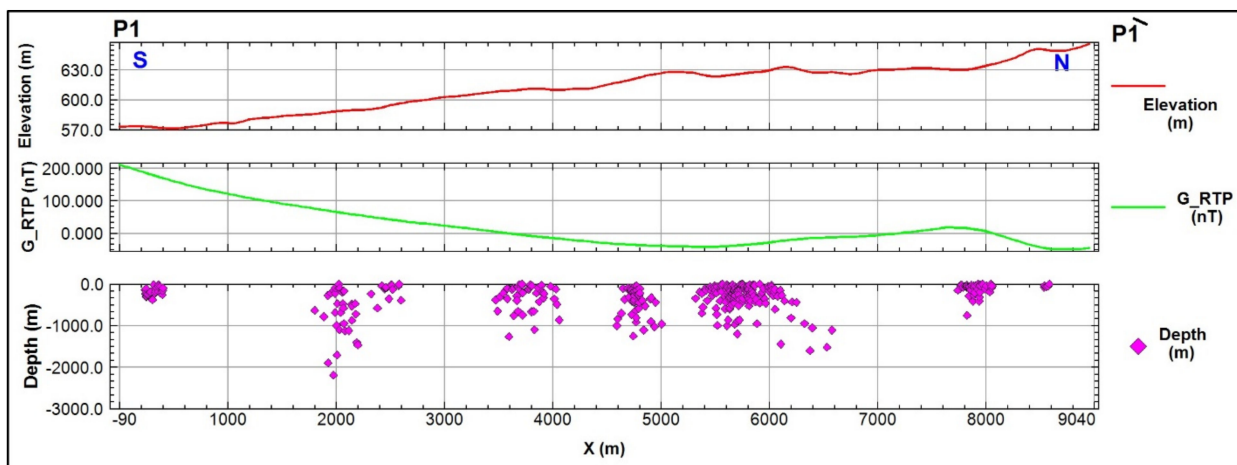

Figure 9. Analytical signal technique for aero magnetic profile (P1) of Homrit Waggat area, Central Eastern Desert, Egypt.
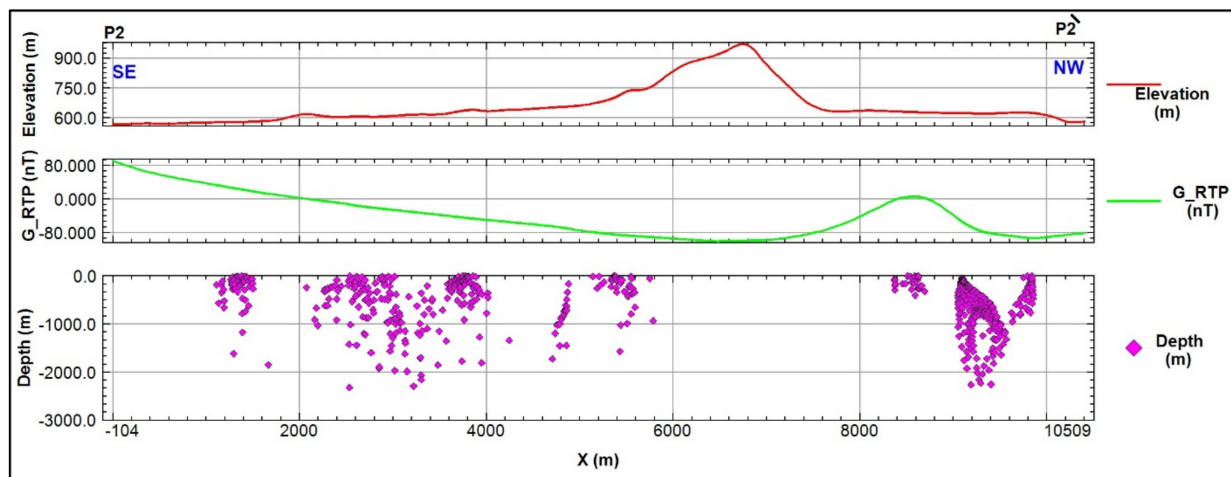
Figure 10. Analytical signal technique for aeromagnetic profile (P2) of Homrit Waggat area, Central Eastern Desert, Egypt.
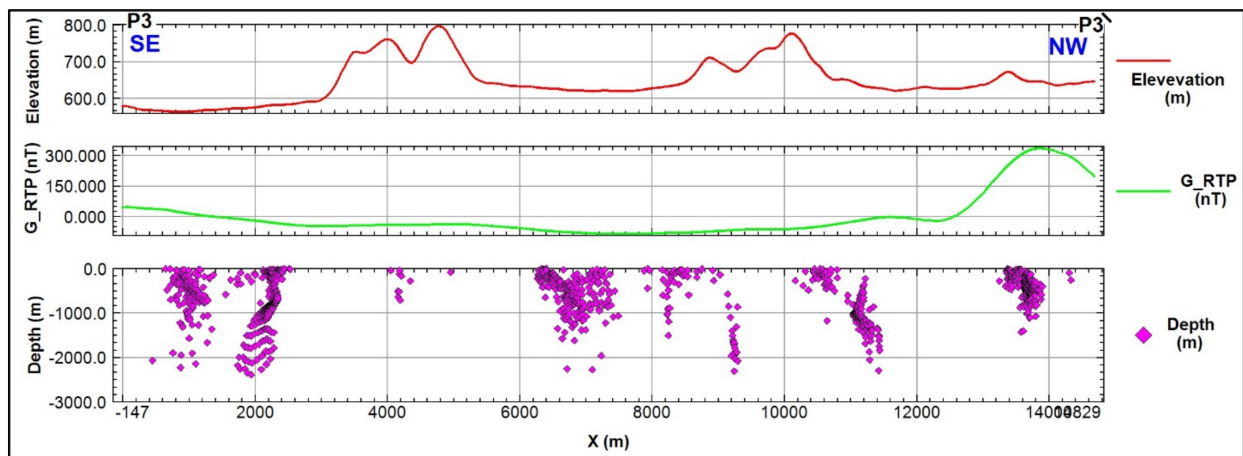

Figure 11. Analytical signal technique for aero magnetic profile (P3) of Homrit Waggat area, Central Eastern Desert, Egypt.

4.7. Euler Deconvolution

Many authors [27–31] have used Euler's differential equation to interpret gravity and magnetic data in terms of simple sources characterized by an integer value of the degree of homogeneity. One major advantage that Euler deconvolution has over other magnetic source location methods is that it is to the orientation of the ambient magnetic field, meaning that it can be used effectively on total-field magnetic anomaly data [28]. The Euler deconvolution technique is carried out by using Oasis montaj, with structural indices (SI) = 0 according to [28]. The solution of the magnetic anomaly maps with SI = 0 for probable subsurface contacts are presented in Figure 12 for the study area. In this figure, there is absolute matching between the Euler clusters and the boundaries of different magnetic anomalies. These boundaries may represent contacts between rock units with different magnetic susceptibilities.
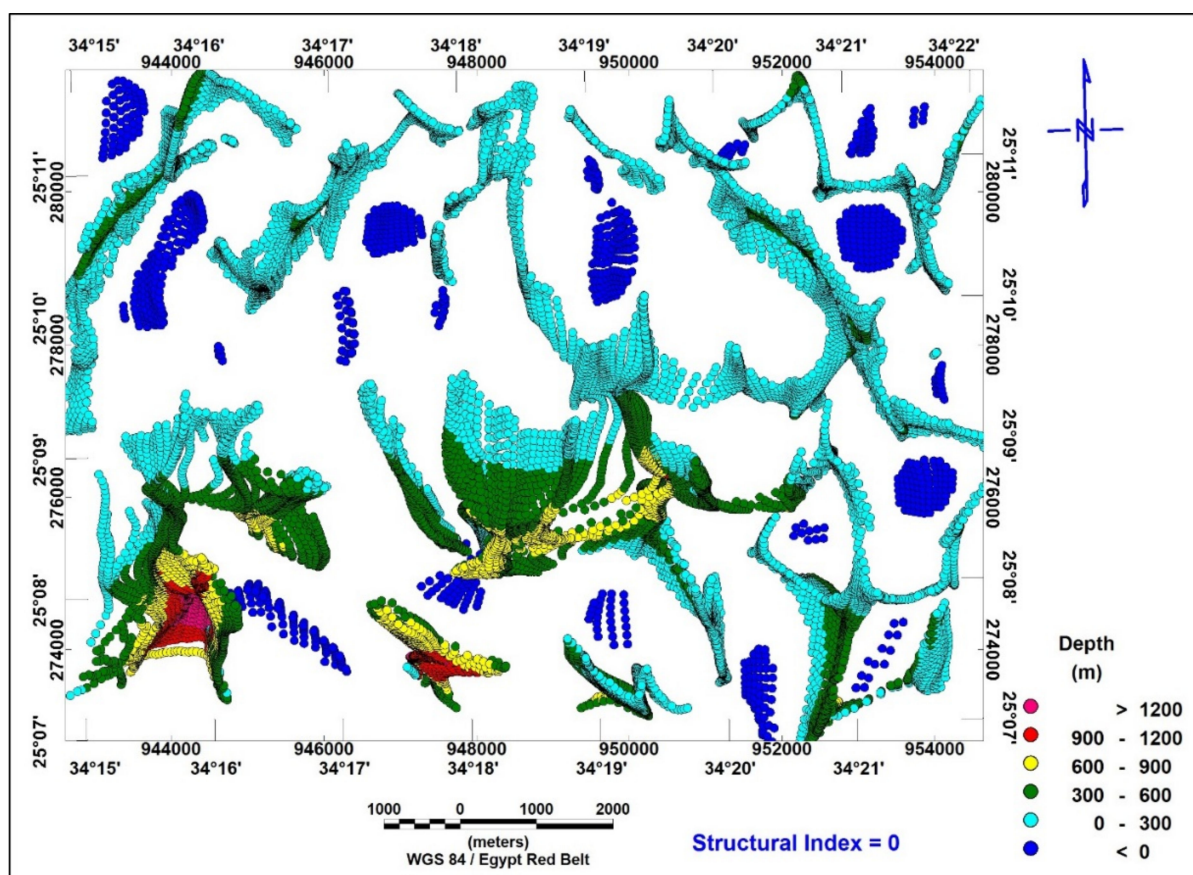
Figure 12. Depth of contacts using Euler deconvolution method (SI = 0) as deduced from RTP map of the study area.

In addition, depth estimation by the 3D Euler deconvolution technique was used for rapid estimation of geologic contacts at different levels in the area under consideration. The zero value structural indexes are used mainly to detect the geological contacts between main lithological units with different magnetic susceptibilities. The reduced to pole map was used as a background to show the matching between the calculated plotted contacts and the boundaries of the magnetic anomalies. The following represents a brief description of the obtained Euler deconvolution map with the value of zero structure index, which is used mainly to detect the geological contacts between central lithological units. The solution contacts map (Figure 12) shows that the subsurface contacts are located at depths ranging between 0 and 1.2 km with major trends of NNW–SSE, NNE–SSW, NE–SW, and N–S. This means that these contacts are located at shallow depths from the surface.

4.8. Structural Setting

Magnetic lineaments are defined as disruptions in the contour patterns, with the disruption caused by association of blocks of rocks of varying composition (of varying magnetic susceptibility) at various places along opposite side of the lineament. The magnetic anomalies are based on the amplitude, wave length, and the shape of contour patterns. We can conclude that trend analysis and the distribution of its pattern can be used to define magnetic provinces which reflect the structural tectonic lineament of the area under study [32]. Trend analysis techniques have been frequently used in various fields of geology and geophysics for purposes of defining structural problems. The interpreted trends are represented by peaks exceeding the significant frequency of the maps. The study area is mainly represented by igneous and sedimentary rocks. These rocks are affected by various regional and local geologic structures of varying types, trends, and locations. The regional and residual magnetic anomaly maps were interpreted to determine the common

structural trends affecting the study area (Figure 13). The subsurface structures in the studied area were traced from the interpreted aeromagnetic maps including the regional and residual maps. The most predominant magnetic fault trends deduced from the analysis of the regional anomaly map have NW–SE, NNE–SSW, NE–SW and N–S trends. On the other hand, the most prominent magnetic fault trends deduced from the analysis of the residual anomaly map have NNE–SSW, NNW–SSE, ESE–WNW and N–S trends. Through the analysis of the regional (deep) and the residual (shallow) anomaly maps, the NW–SE, NNE–SSW and NNW–SSE trends seem to be the most important and significant, and play an effective role in the structural framework of the study area.
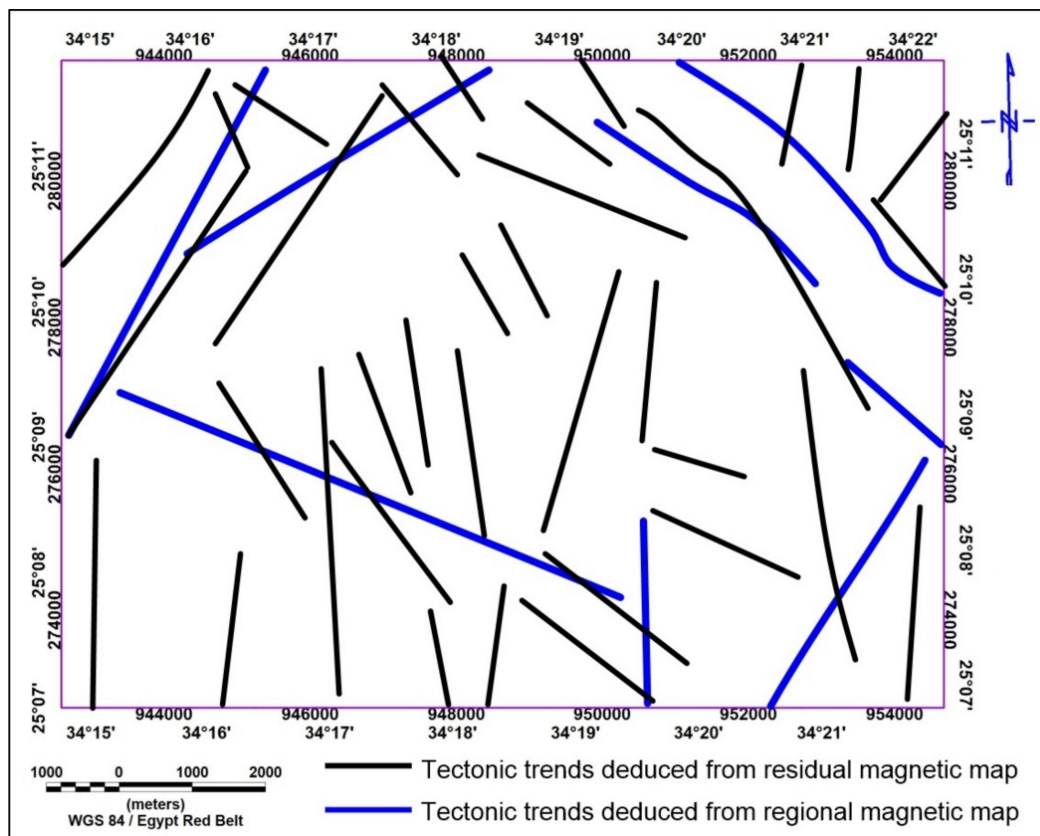

Figure 13. Lineaments as deduced from the regional and residual aeromagnetic map of Homrit Waggat area, Central Eastern Desert, Egypt.

5. Conclusions

Granitic rocks of the Homrit Waggat area form isolated ring-shaped bodies and comprise two granitic subgroups. The first group is the older granitic rocks (tonalite and granodiorite), whereas the second one includes younger granitic rocks (alkali-feldspar granite, syenogranite and albitite granite). The potential field data were subjected to qualitative and quantitative analysis. For the aeromagnetic data, the reduction to the pole approach was used to generate the local structures and anomalous bodies. Filtering was performed to a reduce-to-the-pole (RTP) magnetic map to create two maps: one for the regional component of the magnetic field and the other for the residual component. The generation of a tectonic map for the area under consideration was achieved by combining the results acquired from magnetic data and geological information. The deep-seated magnetic map indicates the presence of numerous sets of structural trends running in four directions, NW–SE, NNE–SSW–NE–SW and N–S, while the shallow zone structural faults trend in the NNE–SSW, NNW–SSE, ESE–WNW and N–S directions, which are consistent with surface structures of previuos work. Using the analytical signal technique, three profiles were generated on the RTP magnetic map to calculate the depth of basement rocks

in the studied area. Depth levels of the economic rare metal-bearing rocks range from 0 km to 1.2 km (Euler deconvolution technique) and from 0 km to 2.3 km (the analytical signal profiles) by using the aeromagnetic data. Therfore, large rare metal-bearing resources occur in Homrit Waggat.

Author Contributions: Conceptualization E.S.R.L.; H.A.A. and A.E.; software E.S.R.L. and W.H.M.; validation H.A.A., A.E., E.S.R.L., W.H.M. and M.K.A. formal analysis, E.S.R.L. and W.H.M.; investigation, E.S.R.L. and W.H.M.; data curation E.S.R.L. and W.H.M. and M.K.A.; writing—original draft preparation, H.A.A., A.E., E.S.R.L. and W.H.M.; writing—review and editing, E.S.R.L., W.H.M.; H.A.A. and A.E., funding acquisition, A.E. All authors have read and agreed to the published version of the manuscript.

Data Availability Statement: The data presented in this study are available on request from the corresponding author.

Conflicts of Interest: The authors declare no conflict of interest.

References

1. Lasheen, E.S.R.; Saleh, G.M.; Khaleal, F.M.; Alwetaishi, M. Petrogenesis of Neoproterozoic Ultramafic Rocks, Wadi Ibib–Wadi Shani, South Eastern Desert, Egypt: Constraints from Whole Rock and Mineral Chemistry. *Appl. Sci.* **2021**, *11*, 10524. [CrossRef]
2. Alzahrani, A.M.; Lasheen, E.S.R.; Rashwan, M.A. Relationship of Mineralogical Composition to Thermal Expansion, Spectral Reflectance, and Physico-Mechanical Aspects of Commercial Ornamental Granitic Rocks. *Materials* **2022**, *15*, 2041. [CrossRef]
3. Kamar, M.S.; Salem, I.A.; El-Aassy, I.E.; El-Sayed, A.A.; Awad, H.A.; Tekin, H.O.; Alzahrai, A.M.; Lasheen, E.S.R. Petrology and Geochemistry of Multiphase Post-Granitic Dikes: A Case Study from the Gabal Serbal Area, Southwestern Sinai, Egypt. *Open Chem.* **2022**, *20*, 169–181. [CrossRef]
4. Saleh, G.M.; Khaleal, F.M.; Lasheen, E.S.R. Geochemistry and Paleoweathering of Metasediments and Pyrite-Bearing Quartzite during the Neoproterozoic Era, Wadi Ibib-Wadi Suwawrib, South Eastern Desert, Egypt. *Arab. J. Geosci.* **2022**, *15*, 51. [CrossRef]
5. Hamdy, M.M.; Lasheen, E.S.R.; Abdelwahab, W. Gold-Bearing Listwaenites in Ophiolitic Ultramafics from the Eastern Desert of Egypt: Subduction Zone-Related Alteration of Neoproterozoic Mantle? *J. Afr. Earth Sci.* **2022**, 104574. [CrossRef]
6. Khaleal, F.M.; Saleh, G.M.; Lasheen, E.S.R.; Alzahrani, A.M.; Kamh, S.Z. Exploration and Petrogenesis of Corundum-Bearing Pegmatites: A Case Study in Migif-Hafafit Area, Egypt. *Front. Earth Sci.* **2022**, *10*, 869828. [CrossRef]
7. Kamar, M.S.; Salem, I.A.; El-Aassy, I.E.; El-Sayed, A.A.; Zakaly, H.M.H.; Alzahrani, A.M.; Lasheen, E.S.R. An Extended Investigation of High-Level Natural Radioactivity and Geochemistry of Neoproterozoic Dokhan Volcanics: A Case Study of Wadi Gebeiy, Southwestern Sinai, Egypt. *Sustainability* **2022**, *14*, 9291. [CrossRef]
8. Lasheen, E.S.R.; Rashwan, M.A.; Osman, H.; Alamri, S.; Khandaker, M.U.; Hanfi, M.Y. Radiological Hazard Evaluation of Some Egyptian Magmatic Rocks Used as Ornamental Stone: Petrography and Natural Radioactivity. *Materials* **2021**, *14*, 7290. [CrossRef]
9. Lasheen, E.S.R.; Azer, M.K.; Ene, A.; Abdelwahab, W.; Zakaly, H.M.H.; Awad, H.A.; Kawady, N.A. Radiological Hazards and Natural Radionuclide Distribution in Granitic Rocks of Homrit Waggat Area, Central Eastern Desert, Egypt. *Materials* **2022**, *15*, 4069. [CrossRef]
10. Abdallah, S.E.; Azer, M.K.; Shammari, A.S.A. The Petrological and Geochemical Evolution of Ediacaran Rare-Metal Bearing A-type Granites from the Jabal Aja Complex, Northern Arabian Shield, Saudi Arabia. *Acta Geol. Sin.-Engl. Ed.* **2020**, *94*, 743–762. [CrossRef]
11. Azer, M.K.; Abdelfadil, K.M.; Asimow, P.D.; Khalil, A.E. Tracking the Transition from Subduction-related to Post-collisional Magmatism in the North Arabian–Nubian Shield: A Case Study from the Homrit Waggat Area of the Eastern Desert of Egypt. *Geol. J.* **2020**, *55*, 4426–4452. [CrossRef]
12. Hadek, H.H.E.; Mohamed, M.A.; Habaak, G.H.E.; Bishara, W.W.; Ali, K.A. Geochemical Constraints on Petrogenesis of Homrit Waggat Rare Metal Granite, Egypt. *Int. J. Geophys. Geochem.* **2016**, *3*, 33–48.
13. Moussa, H.E.; Asimow, P.D.; Azer, M.K.; Abou El Maaty, M.A.; Akarish, A.I.M.; Yanni, N.N.; Mubarak, H.S.; Wilner, M.J.; Elsagheer, M.A. Magmatic and Hydrothermal Evolution of Highly-Fractionated Rare-Metal Granites at Gabal Nuweibi, Eastern Desert, Egypt. *Lithos* **2021**, *400–401*, 106405. [CrossRef]
14. Sami, M.; Mahdy, N.M.; Ntaflos, T.; Fathy, D. Composition and Origin of Ti–Nb–Ta–Zr Bearing Minerals in the Abu Diab Highly Evolved Granite from the Central Eastern Desert of Egypt. *J. Afr. Earth Sci.* **2020**, *165*, 103808. [CrossRef]
15. Abdalla, H.M.; Helba, H.; Matsueda, H. Chemistry of Zircon in Rare Metal Granitoids and Associated Rocks, Eastern Desert, Egypt. *Resour. Geol.* **2009**, *59*, 51–68. [CrossRef]

16.　Parasnis, D.S. *Mining Geophysics*, 2nd ed.; Elsevier Scientific Pub. Comp.: Amsterdam, The Netherlands; Oxford, UK; New York, NY, USA, 1975.

17.　Hassan, M.A.; Hashad, A.H. Precambrian of Egypt. In *The Geology of Egypt*; Said, R., Ed.; Balkema: Rotterdam, The Netherlands, 1990; pp. 201–245.

18.　Silva, A.M.; Pires, A.C.; Mc-Cafferty, A.; Moraes, R. Application of Airborne Geophysical Data to Mineral Exploration in the Uneven Exposed Terrains of the Rio Das Velhas Greenstone Belt. *Rev. Bras. de Geociências* **2003**, *33*, 17–28. [CrossRef]

19.　Li, X. Understanding 3D Analytic Signal Amplitude. *Geophysics* **2006**, *71*, L13–L16. [CrossRef]

20.　MacLeod, I.N.; Jones, K.; Dai, T.F. 3-D Analytic Signal in the Interpretation of Total Magnetic Field Data at Low Magnetic Latitudes. *Explor. Geophys.* **1993**, *24*, 679–687. [CrossRef]

21.　Roest, W.R.; Verhoef, J.; Pilkington, M. Magnetic Interpretation Using the 3-D Analytic Signal. *Geophysics* **1992**, *57*, 116–125. [CrossRef]

22.　Aero-Service. *Final Operational Report of Airborne Magnetic/Radiation Survey in the Eastern Desert, Egypt. For the Egyptian General Pe-Troleum Corporation (EGPC) and the Egyptian Geological Survey and Mining Authority (EGSMA)*; Aero-Service Division: Houston, TX, USA, 1984.

23.　Blakely, R.J. *Potential Theory in Gravity and Magnetic Applications*, 1st ed.; Cambridge University Press: Cambridge, UK, 1995; ISBN 978-0-521-41508-8.

24.　Ammar, A.A.; Fouad, K.M.; Meleik, M.L. Evaluation of the Efficiency of Shortend Low-Pass Filters Computed by Inverse Fourier Transform for Potential Fields of Spherical Bodies and Planar Regionals; Faculty of Earth Sciences. *King Abdulaziz Univ.* **1988**, *1*, 133–148.

25.　Reford, M.S.; Sumner, J.S. Aeromagnetics. *Geophysics* **1964**, *29*, 482–516. [CrossRef]

26.　Milligan, P.R.; Gunn, P.J. Enhancement and Presentation of Airborne Geophysical Data. *J. Aust. Geol. Geophys.* **1997**, *2*, 63–75.

27.　Thompson, D.T. Anew Technique for Making Computer-Assisted Depth Estimates from Magnetic Data. *Geophysics* **1982**, *34*, 31–37. [CrossRef]

28.　Reid, A.B.; Allsop, J.M.; Granser, H.; Millett, A.J.; Somerton, I.W. Magnetic Interpretation in Three Dimensions Using Euler Deconvolution. *Geophysics* **1990**, *55*, 80–91. [CrossRef]

29.　Eshanibli, A.S.; Osagie, A.U.; Ismail, N.A.; Ghanush, H.B. Analysis of Gravity and Aeromagnetic Data to Determine Structural Trend and Basement Depth beneath the Ajdabiya Trough in Northeastern Libya. *SN Appl. Sci.* **2021**, *3*, 228. [CrossRef]

30.　Zhang, C.; Mushayandebvu, M.F.; Reid, A.B.; Fairhead, J.D.; Odegard, M.E. Euler Deconvolution of Gravity Tensor Gradient Data. *GEOPHYSICS* **2000**, *65*, 512–520. [CrossRef]

31.　Cooper, G.R.J. An Improved Algorithm for the Euler Deconvolution of Potential Field Data. *Lead. Edge* **2002**, *21*, 1197–1198. [CrossRef]

32.　Affleck, J. Magnetic anomaly trend and spacing patterns. *Geophysics* **1963**, *28*, 379–395. [CrossRef]